Т. 84, № 1 **ЖУРНАЛ ПРИКЛАДНОЙ СПЕКТРОСКОПИИ** ЯНВАРЬ — ФЕВРАЛЬ 2017
V. 84, N 1 **JOURNAL OF APPLIED SPECTROSCOPY** JANUARY — FEBRUARY 2017

# SOLVENT EFFECTS ON STABILITY, ELECTRONIC STRUCTURE, AND $^{14}$N NQR PARAMETERS OF $Fe(CO)_4py$ ISOMERS**

**R. Ghiasi** [1*], **A. Peikari** [2]

*[1] East Tehran branch, Islamic Azad university, Qiam Dasht, Tehran, Iran;*
*e-mail: rezaghiasi1353@yahoo.com, rghiasi@iauet.ac.ir*
*[2] Young Researchers and Elite Club, Pharmaceutical Science Branch, Islamic Azad University, Tehran, Iran*

*The structure, stability, $^{14}$N NQR parameters, and hyperpolarizability of $Fe(CO)_4py$ isomers in seven different solvents were computed with the MPW1PW91 method based on the polarizable continuum model (PCM). From an energetic standpoint, the $Fe(CO)_4py_{axial}$ isomer was more stable than the $Fe(CO)_4py_{equatorial}$ isomer. On the other hand, the relative energies decreased in more polar solvents. Molecular orbital analysis showed that the HOMO of the $Fe(CO)_4py$ isomer was distributed on the $Fe(CO)_4$ fragment, whereas the LUMO was localized on the pyridine ligand. This study suggests that the nonlinear optical (NLO) properties depend on the solvent polarity.*

***Keyword:*** *$Fe(CO)_4py$ isomers, solvent effect, hyperpolarizability, $^{14}$N NQR parameters.*

# ВЛИЯНИЕ РАСТВОРИТЕЛЕЙ НА СТАБИЛЬНОСТЬ, ЭЛЕКТРОННУЮ СТРУКТУРУ И ЯКР-ПАРАМЕТРЫ ИЗОМЕРОВ $Fe(CO)_4py$

**R. Ghiasi** [1*], **A. Peikari** [2]

*УДК 539.143.43*

*[1] Восточно-Тегеранский филиал Исламского университета Азад, Тегеран, Иран;*
*e-mail: rezaghiasi1353@yahoo.com, rghiasi@iauet.ac.ir*
*[2] Школа молодых исследователей Исламского университета Азад, Тегеран, Иран*

*(Поступила 25 августа 2015)*

*С использованием модели поляризуемого континуума методом MPW1PW91 рассчитаны структура, стабильность, $^{14}$N ЯКР-параметры и гиперполяризуемость изомеров $Fe(CO)_4py$ в различных растворителях. Установлено, что изомер $Fe(CO)_4py_{axial}$ более стабилен, чем $Fe(CO)_4py_{equatorial}$, относительные энергии уменьшаются для более полярных растворителей. Молекулярный орбитальный анализ показывает, что наивысшая молекулярная орбиталь изомера $Fe(CO)_4py$ относится к связи $Fe(CO)_4$, а самая низкая незанятая молекулярная орбиталь локализована на лиганде пиридина. Предполагается, что нелинейные оптические свойства зависят от полярности растворителя.*

***Ключевые слова:*** *изомеры $Fe(CO)_4py$, влияние растворителя, гиперполяризуемость, $^{14}$N ЯКР-параметры.*

**Introduction.** Pentacoordinate transition metal complexes are of exclusive importance in inorganic chemistry. Due to their instability, they are generally involved in the associative reactions of tetracoordinated molecules and the dissociative reactions of hexacoordinate compounds. When pentacoordinate molecules have sufficient stability to be isolated, the distinction between the trigonal bipyramide, the square pyramide, and even other extreme conformations is difficult [1].

The photodissociation of pentacoordinate transition metal carbonyl complexes $Fe(CO)_4L$ was studied theoretically and experimentally [2–4]. Complexes of $Fe(CO)_4L$ (L = pyridine, α- and 7-picoline, piperidine)

---

[**] Full text is published in JAS V. 84, No. 1 (http://springer.com/10812) and in electronic version of ZhPS V. 84, No. 1 (http://www.elibrary.ru/title_about.asp?id=7318; sales@elibrary.ru).

were photochemically synthesized and characterized [5]. The study of the photolysis of [$Fe(CO)_4L$] complexes (L = $NMe_3$ or pyridine) resulted in the formation of $Fe(CO)_3L_{\text{axial}}$ [6]. The reaction is reversed by i.r. light and by annealing the matrix. The $Fe(CO)_3L_{\text{axial}}$ complex isomerizes into $Fe(CO)_3L_{\text{equatorial}}$ after i.r. photolysis.

In this work, we performed a systematic computational study of the solvent effects on the stability, electronic structure, hyperpolarizability, and $^{14}$N NQR parameters of $Fe(CO)_4py$ isomers.

**Computational methods.** All calculations were carried out with Gaussian 03 software [7]. The calculations of the systems containing C, N, O, and H were described by the standard 6-311G(d,p) basis set [8–11]. For iron, the standard LANL2DZ basis set [12–14] was used, and iron was described by the effective core potential of the Wadt-Hay pseudopotential [12] with a double-ξ valence using the LANL2DZ. Geometry optimization was performed using the Modified Perdew-Wang Exchange and Correlation (MPW1PW91) methods [15]. The results of the calculations for transition metal complexes showed that the MPW1PW91 functional gave better results than the B3LYP [16–19]. A vibrational analysis was performed at each stationary point.

Then the geometry of each species in solvents with different dielectric constants was calculated using the polarized continuum model (PCM) [20]. The electrostatic interaction of a nuclear electric quadrupole moment and the electron charge cloud surrounding the nucleus can be used for the observation of pure Nuclear Quadrupole Resonance (NQR) [21]. The Hamiltonian of this interaction for a nucleus of spin I is as follows [22]:

$$H_Q = \frac{e^2Qq_{zz}}{4I(2I-1)}\left[3\hat{I}_z^2 - \hat{I}^2 + (\hat{I}_+^2 + \hat{I}_-^2)\eta/2\right], \tag{1}$$

where all $\hat{I}_+$, $\hat{I}_-$ are the raising and lowering operators, $\hat{I}_z$ is the Z component of the angular momentum operator and $\hat{I}^2$ is the operator for the square of the angular momentum for the nuclei [23]. Quantum chemical calculations yielded the principal components of the electric field gradient (EFG) tensor, $q_{ii}$, in atomic units (1 a.u. = $9.717365 \times 10^{21}$ V/m$^2$) [24], with $|q_{zz}| \geq |q_{yy}| \geq |q_{xx}|$. Here $q_{xx}$, $q_{yy}$ and $q_{zz}$ are the components of EFG in the directions of $x$, $y$, and $z$, respectively. The calculated $q_{ii}$ values were used to obtain the nuclear quadrupole coupling constants, $\chi_{ii}$:

$$\chi_{ii}(\text{MHz}) = e^2Qq_{ii}/h, \quad i = x, y, z, \tag{2}$$

where $Q$ is the nuclear quadrupole moment of the $^{14}$N nucleus. The standard values of quadrupole moment, $Q$, reported by Pyykkö [25] were used in Eq. (1); $Q(^{14}\text{N}) = 20.44$ mb. The NQR parameters were experimentally reported:

$$QCC = \chi\ (\text{MHz}) = e^2Qq_{zz}/h. \tag{3}$$

The asymmetry parameters ($\eta_Q$) were defined as

$$\eta_Q = |(q_{yy} - q_{xx})/q_{zz}|, \quad 0 \leq \eta \leq 1, \tag{4}$$

which determines the deviation of the field gradient tensor from the axial symmetry.

For a nucleus of unit spin (such as $^{14}$N), we had three energy levels, so we got three nuclear quadrupole resonance frequencies [22]:

$$\nu_+ = (3/4)\chi_{zz}(1 + \eta/3)\ , \tag{5}$$

$$\nu_- = (3/4)\chi_{zz}(1 + \eta/3)\ , \tag{6}$$

$$\nu_0 = (3/4)\chi_{zz}\eta. \tag{7}$$

The quadrupole coupling constant ($\chi_{zz}$) and asymmetry parameter ($\eta$) are usually calculated from the nuclear quadrupole frequencies:

$$\chi_{zz} = 2(\nu_+ + \nu_-)/3, \tag{8}$$

$$\eta = 3(\nu_+ - \nu_-)/(\nu_+ + \nu_-). \tag{9}$$

Geometries were optimized without any symmetry constraints, followed by the calculations of the first order hyperpolarizabilities. The first total static hyperpolarizability β was obtained from the relation

$$\beta_{\text{tot}} = \sqrt{\beta_x^2 + \beta_y^2 + \beta_z^2} \tag{10}$$

upon calculating the individual static components

$$\beta_i = \beta_{iii} + \frac{1}{3}\sum_{i \neq j}(\beta_{ijj} + \beta_{jij} + \beta_{jji}) . \qquad (11)$$

The first hyperpolarizability is a third rank tensor that can be represented by a 3 × 3 × 3 matrix. The 27 components of the 3D matrix can be decreased to 10 components because of the Kleinman symmetry [26]:

$$\beta_{xyy} = \beta_{yxy} = \beta_{yyx},\ \beta_{yyz} = \beta_{yzy} = \beta_{zyy}. \qquad (12)$$

So the following equation was employed:

$$\beta_{\text{tot}} = \sqrt{(\beta_{xxx} + \beta_{xyy} + \beta_{xzz})^2 + (\beta_{yyy} + \beta_{yzz} + \beta_{yxx})^2 + (\beta_{zzz} + \beta_{zxx} + \beta_{zyy})^2} . \qquad (13)$$

**Result and discussion.** *Energetic aspects.* Figure 1 represents the structures of the $Fe(CO)_4py_{ax}$ and $Fe(CO)_4py_{eq}$ isomers. The absolute and relative energies of these isomers are listed in Table 1. As shown in Table 1, the $Fe(CO)_4py_{ax}$ isomer is always more stable than the $Fe(CO)_4py_{eq}$ isomer. These values show that the π-acceptor carbonyl ligand tends to occupy the equatorial position [1]. Different solvents essentially affect the ground-state energy gaps ($\Delta E$) between the isomers. The gas phase has the largest ground-state energy gap, which is near 3.40 kcal/mol. The relative energies are less in the solvents than in the gas phase. On the other hand, it was found that these values decrease with increasing the solvents polarity. Figure 2a displays a good linear relationship between the relative energies and the dielectric constants.

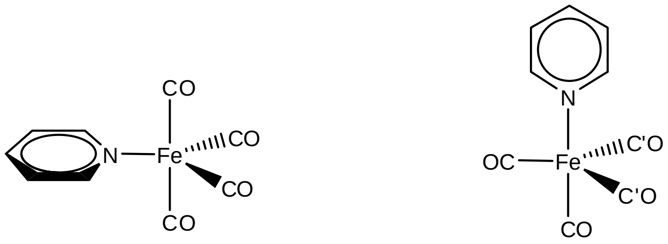

Fig. 1. Structures of $Fe(CO)_4py_{ax}$ and $Fe(CO)_4py_{eq}$ isomers.

TABLE 1. Energy ($E$, Hartree), Relative Energy ($\Delta E$, kcal/mol), Dipole Moment (μ, Debye) of Different Isomers of the $Fe(CO)_4py$ Complex and the Dielectric Constants of Solvents

| Medium | ε | $E$ (equatorial) | $E$(axial) | $\Delta E$ | μ (equatorial) | μ (axial) | Δμ |
|---|---|---|---|---|---|---|---|
| Gas | – | –825.0935 | –825.0989 | 3.40 | 7.17 | 6.44 | 0.72 |
| Chloroform | 4.71 | –825.1003 | –825.1055 | 3.25 | 8.40 | 7.53 | 0.87 |
| Chlorobenzene | 5.70 | –825.1008 | –825.1059 | 3.23 | 8.48 | 7.60 | 0.88 |
| Aniline | 6.89 | –825.1011 | –825.1063 | 3.22 | 8.54 | 7.65 | 0.89 |
| THF | 7.43 | –825.1013 | –825.1064 | 3.22 | 8.57 | 7.67 | 0.90 |
| Methylene chloride | 8.93 | –825.1016 | –825.1067 | 3.20 | 8.62 | 7.72 | 0.91 |
| Quinoline | 9.16 | –825.1016 | –825.1067 | 3.20 | 8.63 | 7.72 | 0.91 |
| Isoquinoline | 11.00 | –825.1019 | –825.1069 | 3.16 | 8.67 | 7.76 | 0.91 |

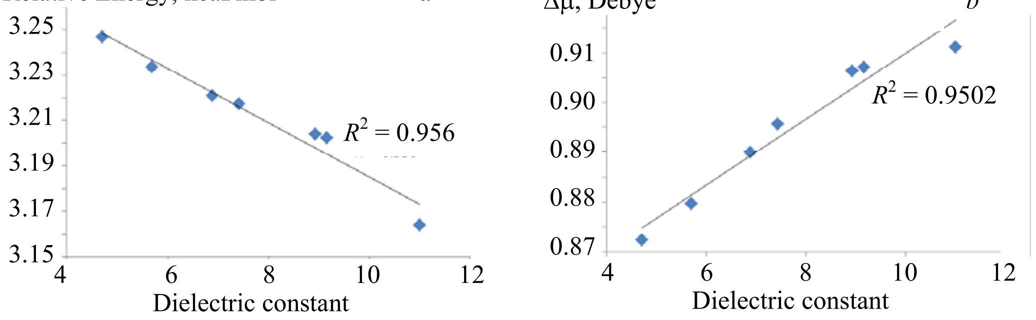

Fig. 2. Linear dependence of relative energies (a) and Δμ (b) on the dielectric constants in $Fe(CO)_4py$ isomers.

*Dipole moments.* The dipole moments of $Fe(CO)_4py_{ax}$ and $Fe(CO)_4py_{eq}$ isomers are listed in Table 1. As seen in Table 1, the $Fe(CO)_4py_{ax}$ molecule has a lesser dipole moment than the $Fe(CO)_4py_{eq}$ isomer. In the liquid phase, dipole moments are greater than in a vacuum. According to the Onsager solvation model, the compound with a greater dipole moment is more stable in polar solvents. On the other hand, it was found that $\Delta\mu = \mu_{\text{eq isomer}} - \mu_{\text{ax isomer}}$ increases with the solvent polarity. Figure 2b represents the dependence of $\Delta\mu$ on the dielectric constants.

*Bond distances.* The selected bond distances of $Fe(CO)_4py_{ax}$ and $Fe(CO)_4py_{eq}$ isomers and the experimental data for the $Fe(CO)_4py_{ax}$ isomer are demonstrated in Table 2. As seen from Table 2, the theoretical results are close to the experimental values for the title molecule, and the minor differences can result from the fact that the theoretical calculations were based on the isolated molecule in the gas phase while the experimental results depicted the molecule in the solid phase. The calculated geometric parameters are in good agreement with the experimental ones, so they can be used as a basis for calculation of the other parameters of the compound.

The structural data for the optimized structures of $Fe(CO)_4py_{ax}$ and $Fe(CO)_4py_{eq}$ isomers in some solvents are represented in Table 2. The results show that the Fe-N bond is slightly longer in the equatorial isomer than in the axial isomer. While the Fe-$C_{ax}$ bonds are longer than the Fe-$C_{eq}$ ones in the equatorial isomer, the Fe-$C_{ax}$ bonds are shorter than the Fe-$C_{eq}$ ones in the axial isomer. These bond length variations are due to the σ-donor ability of the pyridine ligand. Pyridine increases the electron density of the central atom. Owing to this, π-back bonding increases between Fe and CO in cis position to Fe. Therefore, in two isomers carbonyl ligands of cis position to Fe are shorter than those of trans position.

TABLE 2. Selected Structural Parameters of Different Isomers of the $Fe(CO)_4py$ Complex (in Å)

| | | Equatorial isomer | | | | Axial isomer | | |
|---|---|---|---|---|---|---|---|---|
| | ε | Fe-N | Fe-$C_{eq}$ | Fe-$C_{ax}$ | Fe-N | Fe-$C_{eq}$ | Fe-$C_{eq}$(av)* | Fe-$C_{ax}$ |
| Experimental | – | – | – | – | 2.046 | 1.772 | 1.805 | – |
| Gas | – | 2.059 | 1.759 | 1.795 | 2.054 | 1.787 | 1.792 | 1.763 |
| Chloroform | 4.71 | 2.058 | 1.754 | 1.793 | 2.055 | 1.786 | 1.790 | 1.761 |
| Chlorobenzene | 5.70 | 2.058 | 1.754 | 1.793 | 2.055 | 1.786 | 1.790 | 1.761 |
| Aniline | 6.89 | 2.058 | 1.754 | 1.793 | 2.055 | 1.786 | 1.790 | 1.761 |
| THF | 7.43 | 2.058 | 1.754 | 1.793 | 2.054 | 1.786 | 1.790 | 1.761 |
| Methylene chloride | 8.93 | 2.057 | 1.754 | 1.793 | 2.054 | 1.786 | 1.790 | 1.761 |
| Quinoline | 9.16 | 2.057 | 1.754 | 1.793 | 2.054 | 1.786 | 1.790 | 1.761 |
| Isoquinoline | 11.00 | 2.057 | 1.754 | 1.793 | 2.054 | 1.786 | 1.790 | 1.760 |

*The average of Fe-$C_{eq}$ bond lengths.

It is well known that the solvent polarity influences both the structure and properties of conjugated organic molecules and metal complexes [27–29]. But the structural parameters of the studied complexes show that the variations of Fe-C and Fe-N bond lengths change slightly with the polarity of the surrounding media.

*Molecular orbital analysis.* The energies of the frontier orbitals (HOMO, LUMO) along with the corresponding HOMO–LUMO energy gaps for $Fe(CO)_4py_{ax}$ and $Fe(CO)_4py_{eq}$ isomers in a vacuum and a variety of solvents are given in Table 3. As shown in Table 3, the $Fe(CO)_4py_{ax}$ isomer has lower HOMO and LUMO energies than the $Fe(CO)_4py_{eq}$ isomer. Also, the HOMO-LUMO gap and the hardness of the $Fe(CO)_4py_{ax}$ isomer are greater than those of the $Fe(CO)_4py_{eq}$ isomer. As expected from the principles of minimum energy (MEP) and maximum hardness (MHP), when a conformer changes from the most stable to less stable species, the energy increases and the hardness decreases [30–34].

The inclusion of the solvation effects leads to changes in the molecular orbital energies (Table 3). In the solution, HOMO is stabilized, but LUMO is unstabilized, with respect to the corresponding values in a vacuum. Figure 3a shows the dependence of the frontier orbitals energies on the dielectric constant. Figure 3b represents the plots of HOMO and LUMO for $Fe(CO)_4py$ isomers. It can be found that the HOMO of $Fe(CO)_4py$ isomers is distributed on the $Fe(CO)_4$ fragment, but LUMO is localized on the pyridine ligand.

*$^{14}$N-NQR parameters.* The distortion of the charge distributions around the nitrogen atom was investigated and interpreted by EFGs. Since the EFG around a nitrogen nucleus is symmetric in the $N_2$ free molecule, the calculated NQR parameters for the $N_2$ molecule are $\eta_Q = 0$ and $\nu_Q^{cal} = 4.258$ MHz. The calculated NQR frequencies of the nitrogen atoms in $Fe(CO)_4py$ isomers in the gas phase and different solvents are

listed in Table 4. As shown in Table 4, the magnitude of the $q_{zz}$, $\chi_{zz}$ and $\eta$ values decreases more in the solution phase than in a vacuum. On the other hand, $\nu_+$, $\nu_-$, and $\nu_0$ frequencies are dependent on the polarity of the solvents. Figure 4 represents a good linear relationship between these values and the dielectric constants. A comparison of the $q_{zz}$, $\chi_{zz}$, and $\eta$ values of the isomers shows that these values are larger in the equatorial isomer than in the axial isomer. There is a good relationship between $\Delta\eta$ and $\Delta\chi_{zz}$ and the relative energies of the isomers:

$$\Delta\chi_{zz} = 0.0926\Delta E - 0.0501;\ R^2 = 0.8881,$$
$$\Delta\eta = -0.0278\Delta E + 0.1059;\ R^2 = 0.9259.$$

TABLE 3. Frontier Orbitals Energies (eV), HOMO-LUMO Gap Energy ($\Delta E$, eV), Hardness ($\eta$, eV), Chemical Potential ($\mu$, eV), and Electrophilicity ($\omega$, eV) Values of Different Isomers of the Fe(CO)$_4$py Complex

| Medium | $E_{\text{HOMO}}$ | $E_{\text{LUMO}}$ | $\Delta E$ | $\eta$ | $\mu$ | $\omega$ | $E_{\text{HOMO}}$ | $E_{\text{LUMO}}$ | $\Delta E$ | $\eta$ | $\mu$ | $\omega$ |
|---|---|---|---|---|---|---|---|---|---|---|---|---|
| | *Axial isomer* | | | | | | *Equatorial isomer* | | | | | |
| Gas | –6.09 | –1.90 | 4.19 | 2.10 | –4.00 | 3.81 | –5.84 | –1.85 | 3.99 | 2.00 | –3.85 | 3.71 |
| Chloroform | –6.21 | –1.61 | 4.60 | 2.30 | –3.91 | 3.32 | –5.95 | –1.53 | 4.42 | 2.21 | –3.74 | 3.17 |
| Chlorobenzene | –6.22 | –1.59 | 4.63 | 2.31 | –3.90 | 3.29 | –5.96 | –1.52 | 4.45 | 2.22 | –3.74 | 3.14 |
| Aniline | –6.22 | –1.58 | 4.65 | 2.32 | –3.90 | 3.27 | –5.98 | –1.50 | 4.48 | 2.24 | –3.74 | 3.12 |
| THF | –6.23 | –1.57 | 4.66 | 2.33 | –3.90 | 3.26 | –5.98 | –1.49 | 4.48 | 2.24 | –3.74 | 3.11 |
| Methylene chloride | –6.23 | –1.56 | 4.67 | 2.34 | –3.90 | 3.25 | –5.98 | –1.48 | 4.50 | 2.25 | –3.73 | 3.10 |
| Quinoline | –6.23 | –1.56 | 4.67 | 2.34 | –3.90 | 3.25 | –5.98 | –1.48 | 4.50 | 2.25 | –3.73 | 3.09 |
| Isoquinoline | –6.24 | –1.55 | 4.69 | 2.34 | –3.89 | 3.23 | –5.99 | –1.47 | 4.52 | 2.26 | –3.73 | 3.08 |

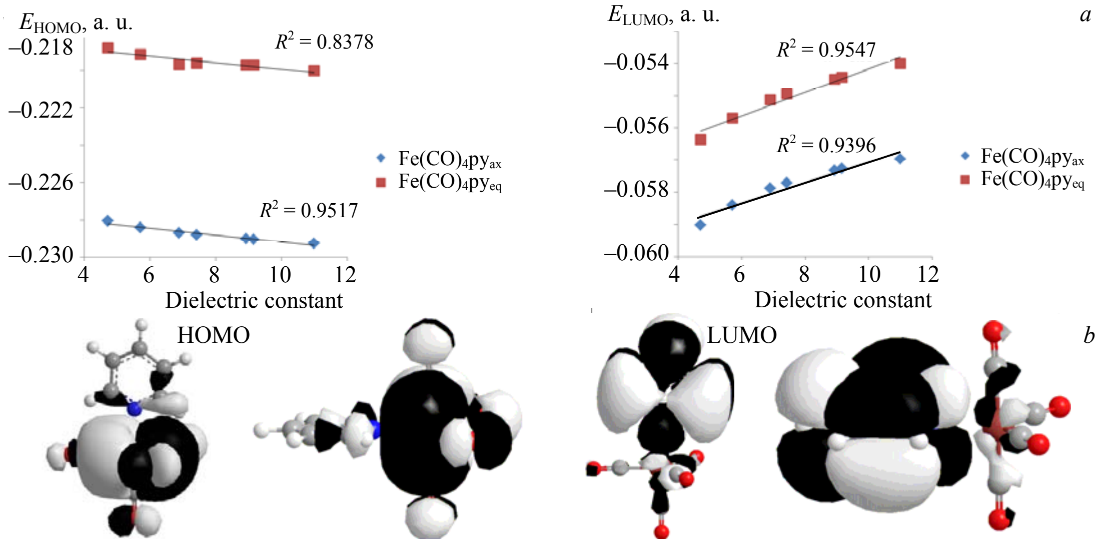

Axial isomer Equatorial isomer Axial isomer Equatorial isomer

Fig. 3. Linear dependence of the frontier orbital energies on the dielectric constants (a) and the frontier orbitals of Fe(CO)$_4$py isomers (b).

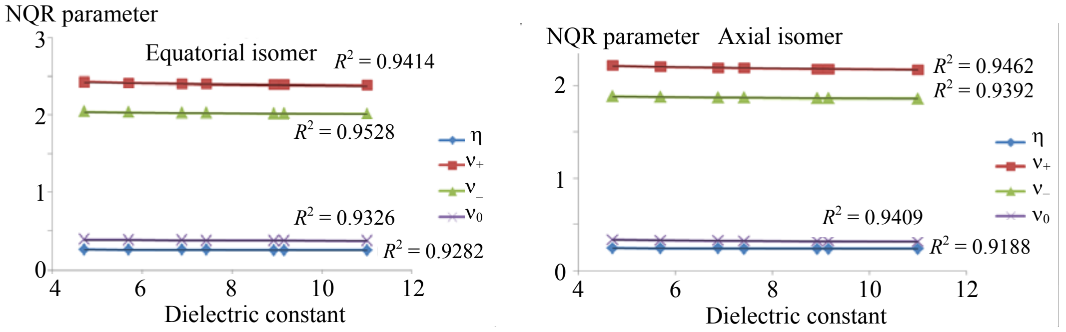

Fig. 4. Linear dependence of NQR parameters on the dielectric constants of Fe(CO)$_4$py isomers.

TABLE 4. $^{14}$N NQR Parameters of Different Isomers of the $Fe(CO)_4py$ Complex in Different Media Using the PCM Model

| Solvent | $q_{xx}$, a.u | $q_{yy}$, a.u | $q_{zz}$, a.u | $(e^2Q/h)q_{xx}$ | $(e^2Q/h)q_{yy}$ | $(e^2Q/h)q_{zz}$ | η | $\nu_+$ | $\nu_-$ | $\nu_0$ |
|---|---|---|---|---|---|---|---|---|---|---|
| *Axial isomer* | | | | | | | | | | |
| Gas | –0.219 | –0.395 | 0.615 | –1.054 | –1.898 | 2.952 | 0.286 | 2.425 | 2.003 | 0.422 |
| Chloroform | –0.215 | –0.354 | 0.569 | –1.031 | –1.700 | 2.731 | 0.245 | 2.215 | 1.881 | 0.335 |
| Chlorobenzene | –0.214 | –0.351 | 0.566 | –1.029 | –1.687 | 2.717 | 0.242 | 2.202 | 1.873 | 0.329 |
| Aniline | –0.214 | –0.349 | 0.563 | –1.028 | –1.677 | 2.705 | 0.240 | 2.191 | 1.866 | 0.325 |
| THF | –0.214 | –0.348 | 0.562 | –1.027 | –1.673 | 2.700 | 0.239 | 2.187 | 1.864 | 0.323 |
| Methylene chloride | –0.214 | –0.347 | 0.560 | –1.026 | –1.665 | 2.691 | 0.237 | 2.178 | 1.859 | 0.319 |
| Quinoline | –0.214 | –0.346 | 0.560 | –1.026 | –1.664 | 2.690 | 0.237 | 2.177 | 1.858 | 0.319 |
| Isoquinoline | –0.213 | –0.345 | 0.559 | –1.025 | –1.657 | 2.682 | 0.236 | 2.170 | 1.854 | 0.316 |
| *Equatorial isomer* | | | | | | | | | | |
| Gas | –0.236 | –0.435 | 0.670 | –1.132 | –2.087 | 3.219 | 0.297 | 2.653 | 2.175 | 0.478 |
| Chloroform | –0.229 | –0.391 | 0.620 | –1.101 | –1.878 | 2.979 | 0.261 | 2.429 | 2.040 | 0.388 |
| Chlorobenzene | –0.229 | –0.388 | 0.617 | –1.099 | –1.865 | 2.964 | 0.258 | 2.415 | 2.032 | 0.383 |
| Aniline | –0.229 | –0.386 | 0.615 | –1.098 | –1.855 | 2.953 | 0.257 | 2.404 | 2.025 | 0.379 |
| THF | –0.228 | –0.385 | 0.614 | –1.097 | –1.851 | 2.947 | 0.256 | 2.399 | 2.022 | 0.377 |
| Methylene chloride | –0.228 | –0.384 | 0.612 | –1.096 | –1.842 | 2.938 | 0.254 | 2.390 | 2.017 | 0.373 |
| Quinoline | –0.228 | –0.383 | 0.611 | –1.095 | –1.841 | 2.936 | 0.254 | 2.389 | 2.016 | 0.373 |
| Isoquinoline | –0.228 | –0.382 | 0.610 | –1.093 | –1.835 | 2.929 | 0.253 | 2.382 | 2.011 | 0.371 |

*Hyperpolarizability.* It is illustrated that the solvent polarity plays an important role in the first hyperpolarizability of the dipolar molecules. The $\beta_{tot}$, $\beta_x$, $\beta_y$, $\beta_z$ values of $Fe(CO)_4py$ isomers in a variety of solvents is listed in Table 5. These values indicate that $\beta_{tot}$ decreases from a vacuum to the solution phase. The dependence of the first hyperpolarizability of the studied compound both on the dielectric constant of the media and the Onsager function was investigated [35]. Figure 5 is typical for a dipolar reaction field interaction in the salvation process [35–38]. Therefore, the electronic reorganization in the solution for $Fe(CO)_4py$ has an important effect on the resulting first hyperpolarizability. From Table 5, in the equatorial isomer, the $\beta_x$ values dominate the nonlinear optical (NLO) response, because the skeleton atoms are mostly located on the $x$-axis, and the variation tendency of the $\beta_z$ and $\beta_x$ values for this isomer is close to zero. On the other hand, in the axial isomer, the $\beta_z$ values dominate the NLO response, because the skeleton atoms are mostly located on the $z$-axis. The $\beta_x$ values also notably contribute to the NLO responses, and the $\beta_y$ values for this isomer are close to 0.1. The resulting isomer of the substitution of the equatorial carbonyl ligand in the $Fe(CO)_5$ molecule with the pyridine ligand has a more symmetric structure than the substitution in the axial position. Therefore, this structure is sufficient for revealing the relationship between the $\beta_x$ value and the geometrical structure. For the axial isomer, due to the change of the pyridine location, there is an increase in the $\beta_{tot}$ values. This shows that the NLO responses could be tuned by changing the location of pyridine.

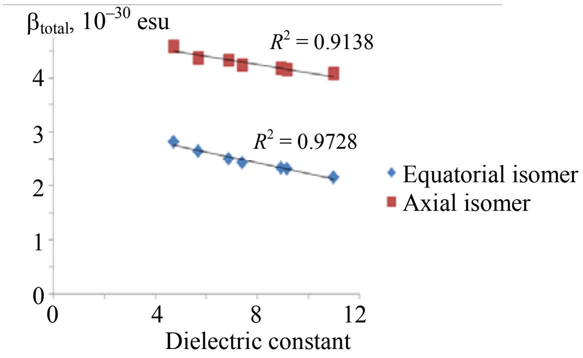

Fig. 5. Linear dependence of $\beta_{total}$ on the dielectric constants of $Fe(CO)_4py$ isomers.

TABLE 5. $\beta_{tot}$, $\beta_x$, $\beta_y$, and $\beta_z$ Values (×$10^{-30}$ esu) for Different Isomers of the $Fe(CO)_4py$ Complex in Different Media Using the PCM Model

| | Gas | Chloroform | Chlorobenzene | Aniline | THF | Methylene chloride | Quinoline | Isoquinoline |
|---|---|---|---|---|---|---|---|---|
| *Axial isomer* | | | | | | | | |
| $\beta_x$ | 1.88 | 1.13 | –0.68 | 0.97 | –0.78 | 0.89 | 0.88 | 0.84 |
| $\beta_y$ | 0.02 | –0.09 | –0.09 | –0.10 | –0.10 | –0.10 | –0.10 | –0.10 |
| $\beta_z$ | 5.78 | 4.45 | 4.33 | 4.22 | 4.18 | 4.08 | 4.07 | 3.99 |
| $\beta_{tot}$ | 6.08 | 4.59 | 4.38 | 4.33 | 4.25 | 4.18 | 4.16 | 4.08 |
| *Equatorial isomer* | | | | | | | | |
| $\beta_x$ | –4.25 | 2.81 | 2.64 | 2.50 | 2.43 | 2.32 | 2.31 | –2.15 |
| $\beta_y$ | –0.02 | 0.01 | 0.01 | 0.02 | 0.02 | 0.02 | 0.02 | 0.01 |
| $\beta_z$ | –0.01 | –0.03 | –0.02 | –0.03 | –0.03 | –0.01 | –0.01 | –0.02 |
| $\beta_{tot}$ | 4.25 | 2.81 | 2.64 | 2.50 | 2.43 | 2.32 | 2.31 | 2.15 |

**Conclusion.** In this work, a theoretical investigation of the solvent effect on the structures, stability, $^{14}N$ NQR parameters, and hyperpolarizability of $Fe(CO)_4py$ isomers in different solvents shows that (i) the $Fe(CO)_4py_{axial}$ is more stable than the $Fe(CO)_4py_{equatorial}$ isomer; (ii) the relative energy values decrease with increasing polarity of solvents; (iii) the HOMO of $Fe(CO)_4py$ isomer is distributed on the $Fe(CO)_4$ fragment, and the LUMO is localized on the pyridine ligand; (iv) a comparison of the $\chi_{zz}$ and $\eta$ values of the isomers show that these values are larger in the equatorial isomer than the axial isomer; (v) the hyperpolarizability increases more in a vacuum than in the solution phase.

## REFERENCES

1. A. R. Rossi, R. Hoffmann, *Inorg. Chem.*, **14**, 365–374 (1975).
2. T. P. M. Goumans, A. W. Ehlers, M. C. V. Hemert, A. Rosa, E.-J. Baerends, K. Lammertsma, *J. Am. Chem. Soc.*, **125**, 3558–3567 (2003).
3. S. P. Modi, J. D. Atwood, *Inorg. Chem.*, **22**, 26–28 (1983).
4. J. A. S. Howell, M. G. Palin, P. McArdle, D. Cunningham, Z. Goldschmidt, H. E. Gottlieb, D. H.-Langermans, *Inorg. Chem.*, **32**, 3493–3500 (1993).
5. E. H. Shubert, R.K. Sheline, *Inorg. Chem.*, **5**, 1071–1074 (1966).
6. G. Boxhoorn, M. B. Cerfontain, D. J. Stufkens, A. Oskam, *J. Chem. Soc., Dalton Trans.*, 1336–1341 (1980).
7. *Gaussian 03*, Gaussian Inc., Pittsburgh, PA (2003).
8. R. Krishnan, J. S. Binkley, R. Seeger, J. A. Pople, *J. Chem. Phys.*, **72**, 650–654 (1980).
9. P. J. Hay, *J. Chem. Phys.*, **66**, 4377–4384 (1977).
10. A. D. McLean, G. S. Chandler, *J. Chem. Phys.*, **72**, 5639–5648 (1980).
11. A. J. H. Wachters, *J. Chem. Phys.*, **52**, 1033–1036 (1970).
12. P. J. Hay, W. R. Wadt, *J.Chem.Phys.*, **82**, 299–310 (1985).
13. P. J. Hay, W. R. Wadt, *J.Chem.Phys.*, **82**, 284–298 (1985).
14. A. Schaefer, H. Horn, R. Ahlrichs, *J. Chem. Phys*, **97**, 2571–2577 (1992).
15. C. Adamo, V. Barone, *J. Chem. Phys.*, **108**, 664–675 (1998).
16. M. Porembski, J. C. Weisshaar, *J. Phys. Chem. A*, **105**, 6655–6667 (2001).
17. Y. Zhang, Z. Guo, X.-Z. You, *J. Am. Chem. Soc.*, **123**, 9378–9387 (2001).
18. R. C. Dunbar, *J. Phys. Chem. A*, **106**, 7328–7337 (2002).
19. J. P. C. A. M. Porembski, J. C. Weisshaar, *J. Phys. Chem. A*, **105**, 4851–4864 (2001).
20. J. Tomasi, B. Mennucci, R. Cammi, *Chem. Rev.*, **105**, 2999–3093 (2005).
21. J. D. Graybeal, *Molecular Spectroscopy*, McGraw-Hill (1988).
22. J. Seliger, *Nuclear Quadrupole Resonance, Theory – Encyclopedia of Spectroscopy and Spectrometry*, Academic Press (2000).
23. C. P. Slichter, *Principles of Magnetic Resonance*, 3rd ed., Springer-Verlag, Heidelberg (1990).
24. T. P. Das, E. L. Hahn, *Solid State Physics*, New York (1958).
25. M. Tokman, D. Sundholm, P. Pyykkö, J. Olsen, *Chem. Phys. Lett.*, **265**, 60–64 (1997).
26. D. A. Keleiman, *Phy. Rev.*, **129**, 1977–1979 (1962).

27. P. J. Mendes, T. J. L. Silva, A. J. P. Carvalho, J. P. P. Ramalho, *J. Mol. Struct.: THEOCHEM*, **946**, 33–42 (2010).
28. L. M. Chen, J. C. Chen, H. Luo, et. al., *J. Theor. Comput. Chem.*, **10**, 581–604 (2011).
29. X. Cao, C. Liu, Y. Liu, *J. Theor. Comput. Chem.*, **11**, 573–586 (2012).
30. P. W. Ayers, R. G. Parr, *J. Am. Chem. Soc.*, **122**, 2010–2018 (2000).
31. R. G. Parr, P. K. Chattaraj, *J. Am. Chem. Soc.*, **113**, 1854–1855 (1991).
32. R. G. Pearson, *J. Chem. Educ.*, **64**, 561–567 (1987).
33. R. G. Pearson, *Acc. Chem. Res.* , **26**, 250–255 (1993).
34. R. G. Pearson, *J. Chem. Educ.*, **76**, 267–270 (1999).
35. L. Onsager, *J. Am. Chem. Soc.*, **58**, 1486–1493 (1936).
36. K. Clays, A. Persoons, *Phys. Rev. Lett.*, **66**, 2980–2983 (1991).
37. P.C. Ray, J. Leszczynsk, *Chem. Phys. Lett.*, **399**, 162–166 (2004).
38. H. Lee, S.-Y. An, M. Cho, *J. Phys. Chem. B*, **103**, 4992–4996 (1999).